

Biochemical and Structural Analysis of Common Cancer-Associated KRAS Mutations

John C. Hunter, Anuj Manandhar, Martin A. Carrasco, Deepak Gurbani, Sudershan Gondi, and Kenneth D. Westover

Abstract

KRAS mutations are the most common genetic abnormalities in cancer, but the distribution of specific mutations across cancers and the differential responses of patients with specific KRAS mutations in therapeutic clinical trials suggest that different KRAS mutations have unique biochemical behaviors. To further explain these high-level clinical differences and to explore potential therapeutic strategies for specific KRAS isoforms, we characterized the most common KRAS mutants biochemically for substrate binding kinetics, intrinsic and GTPase-activating protein (GAP)-stimulated GTPase activities, and interactions with the RAS effector, RAF kinase. Of note, KRAS G13D shows rapid nucleotide exchange kinetics compared with other mutants analyzed. This property can be

explained by changes in the electrostatic charge distribution of the active site induced by the G13D mutation as shown by X-ray crystallography. High-resolution X-ray structures are also provided for the GDP-bound forms of KRAS G12V, G12R, and Q61L and reveal additional insight. Overall, the structural data and measurements, obtained herein, indicate that measurable biochemical properties provide clues for identifying KRAS-driven tumors that preferentially signal through RAF.

Implications: Biochemical profiling and subclassification of KRAS-driven cancers will enable the rational selection of therapies targeting specific KRAS isoforms or specific RAS effectors. *Mol Cancer Res*; 13(9); 1325–35. ©2015 AACR.

Introduction

RAS genes were the first oncogenes identified (1, 2) and now, in the age of detailed genetic tumor characterization, they have ultimately proven to be the most commonly mutated of all discovered oncogenes with approximately 30% of tumors containing RAS mutations (3–5). In 2013, the American Cancer Society estimated the number of new cancers in the United States to be approximately 1.6 million (6). Combining estimates of RAS mutation frequencies with raw cancer numbers suggests that, in 2013, hundreds of thousands of persons in the United States presented with RAS-mutated cancers, including mutations in the RAS family members NRAS, HRAS and, most commonly (~85% of all RAS mutations), Kirsten rat sarcoma viral oncogene homolog (KRAS).

Early efforts to correlate the biochemical consequences of RAS mutations with manifestations of human disease focused primarily on HRAS and were able to show connections between specific mutations and cell transformability, but these did not translate into clinical predictors (7, 8). Several decades later, we now appreciate that RAS biology is far more complex and context-

dependent than was understood at that time, likely requiring more sophisticated experimental designs to begin to understand how RAS mutants behave differentially in biology. Furthermore, despite the high degree of sequence similarity between HRAS and KRAS, the observations made using HRAS may not necessarily apply to KRAS (9). These concepts, coupled with a renewed enthusiasm around the idea of targeting KRAS (10) have motivated us to study the critical question—Are the biologic behaviors of specific KRAS mutations measurably different and is it possible to subclassify specific KRAS-containing tumors based on biochemical behavior?

Several key observations suggest that specific KRAS mutations have unique biologic and clinical behaviors. The first is that specific KRAS mutations are more common in specific tumor types. For example, KRAS mutations are enriched in relatively common and life-threatening cancers, such as pancreatic cancer (70%–90% of cases), colon cancer (35%–50%), small intestinal cancer (35%), biliary cancer (20%–30%), and lung cancer (20%–35%; ref. 10), while NRAS mutations are most common in hematopoietic/lymphoid (10%) and skin cancers and HRAS mutations dominant in cervical (9%) and salivary gland tumors (15%). Furthermore, within these cancers, specific KRAS mutations dominate. For example, KRAS G12D is the most common mutation in pancreatic (two thirds of KRAS mutations) and colorectal (almost half of KRAS mutations), while KRAS G12C is most common in lung cancer (half of KRAS mutations; ref. 11). The forces driving these differences have been explored and are likely a combination of the nature of the genotoxic stress causing the mutations (12, 13) and biologic selection with influence from many factors ranging from genomic topology, (14, 15) to protein expression levels (16, 17), and cellular context (5, 18, 19). Consistent with the idea that specific KRAS mutations confer unique biologic properties, it now

Departments of Biochemistry and Radiation Oncology, The University of Texas Southwestern Medical Center at Dallas, Dallas, Texas.

Note: Supplementary data for this article are available at Molecular Cancer Research Online (<http://mcr.aacrjournals.org/>).

Corresponding Author: Kenneth D. Westover, The University of Texas Southwestern Medical Center, 5323 Harry Hines Boulevard, L4.268, Dallas, TX 75390-9038. Phone: 214-645-0323; Fax: 214-645-7622; E-mail: kenneth.westover@utsouthwestern.edu

doi: 10.1158/1541-7786.MCR-15-0203

©2015 American Association for Cancer Research.

Hunter et al.

appears that some mutations of KRAS may also be prognostic (20–25) and predictive (21, 26) in selected settings.

RAS is a guanine nucleotide binding protein that is typically found at the inner leaflet of the cell membrane by virtue of a posttranslational lipid modification at its C-terminus. It operates in key signaling pathways as a molecular switch, becoming activated when bound to GTP but is inactive when bound to GDP. In normal physiology, conversion from GDP to GTP-bound state happens when growth factors bind to extracellular receptors, inducing nucleotide exchange with the help of guanine nucleotide (27) exchange factors (GEF), such as Son of sevenless (SOS) that pry open RAS allowing GDP to dissociate and GTP to bind (28). Alternatively, conversion from GTP to GDP happens through a GTPase activity intrinsic to RAS, which is greatly stimulated by GTPase-activating proteins (GAP; ref. 29). GTP-bound (activated) RAS passes signals based on a specific conformation characterized by "closure" of two dynamic structural elements called switch 1 and switch 2 around GTP. This conformation is controlled by several interactions, including those between the residues T35 and G60 with the gamma phosphate of GTP. The closed RAS conformation is competent to interact with RAS "effectors," such as RAF kinases and PI3K, which propagate and amplify signals from RAS (30, 31). Cancer-causing mutations in RAS or other members of the pathway result in a higher likelihood that RAS is GTP bound and are often related to impairment of intrinsic or GAP-stimulated hydrolysis of GTP (32). Regulators (GEFs and GAPs) of RAS and RAS effectors all share the commonality of interacting with the switches. One of the valuable insights gained by combining the available tumor sequencing data and RAS structural data is that most cancer-associated RAS mutations are either within the switches or at locations that would be expected to influence enzymatic activity.

The signaling pathways that receive input from KRAS are notably complex and in many cases interconnected (33). It is possible that certain mutant isoforms of KRAS preferentially signal through particular pathways over others. If such patterns could be identified, it would provide a rationale for selecting patients for therapies that target certain downstream RAS pathways. In addition, we hypothesized that biochemical measurements may aid in the design of direct isoform-specific therapeutic strategies. As a first step, here we

profile the biochemical and biophysical properties of commonly occurring mutant forms of KRAS (G12A, G12C, G12D, G12R, G12V, G13D, Q61L, and Q61H), including the intrinsic and GAP-stimulated GTP hydrolysis rates, GTP and GDP-binding kinetics measurements, relative affinities for RAF kinase, and high-resolution crystal structures. Using these data, we propose a KRAS mutation categorization scheme that we evaluate in the context of publicly available clinical tumor data.

Materials and Methods

Protein expression and purification

Protein was expressed and purified as described previously (34) and is outlined in detail in Supplementary Materials and Methods. An expression construct encoding the catalytic domain (residues 714–1047) of RASA1 (P120GAP) was a gift from Xuewu Zhang (Departments of Pharmacology and Biophysics, The University of Texas Southwestern Medical Center at Dallas, Dallas, Texas). The cDNA sequence of RAS-binding domain (RBD) of RAF-1 kinase (residues 51–91) with a C-terminal TEV cleavable 6Xhis tag was synthesized (Mr. Gene) and cloned into a pTriEx expression vector. Expression and purification of P120GAP and RAF-RBD were performed as described for KRAS. Protein was buffer exchanged into 20 mmol/L Tris pH 8.0, 50 mmol/L NaCl, 1 mmol/L DTT, and stored at -80°C until use.

Nucleotide exchange assay

KRAS protein was loaded with GDP and protein concentration adjusted to 45 $\mu\text{mol/L}$ (1 mg/mL) with 20 mmol/L Tris, 150 mmol/L NaCl. KRAS protein at a final concentration of 750 nmol/L was mixed with 1.5 $\mu\text{mol/L}$ mant-GTP or mant-GDP (in 20 mmol/L Tris, 50 mmol/L NaCl, 10 mmol/L MgCl_2 , 20 mmol/L EDTA) in a 4-mL cuvette. Fluorescence was measured every 1 second for 15 minutes at excitation/emission set to 360 nm/440 nm in a Synergy Neo reader (BioTek). Data were exported and analyzed using GraphPad Prism (GraphPad Software, Inc.). All readings were performed in triplicate.

GTPase assay

GTPase activity was measured using EnzCheck phosphate assay system (Life Technologies) to continuously measure

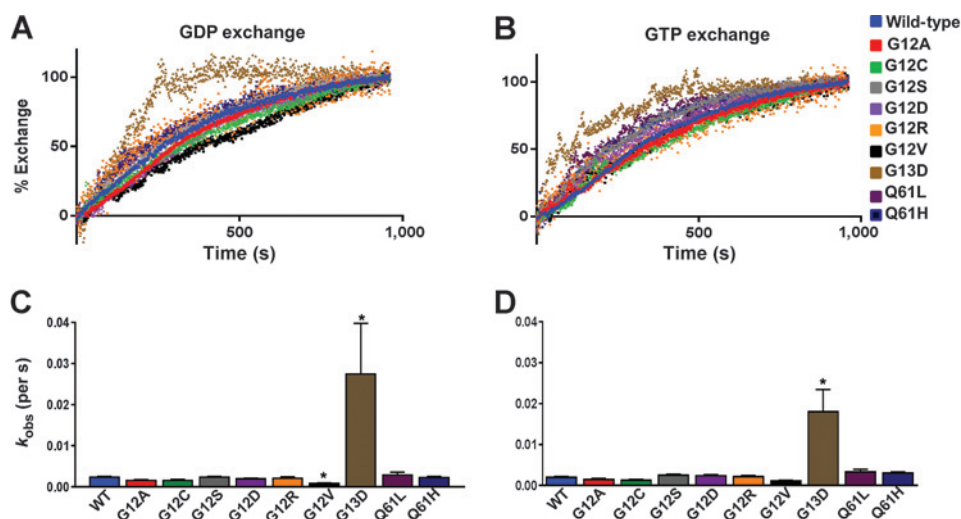


Figure 1. Nucleotide exchange kinetics of KRAS mutants. A and B, GDP-loaded KRAS was incubated with an excess of mant-GDP (A) or mant-GTP (B) and the rate of exchange followed as a function of change in fluorescence over time. C, first-order rate constants were determined for each mutant. Rates (mean of three independent measurements) for GDP are shown with black bars and GTP with white \pm SEM. †, Indicates a statistically significant difference compared with WT KRAS ($P < 0.01$).

phosphate release following the manufacturer's recommended protocol. Briefly, KRAS proteins in assay buffer (30 mmol/L Tris, pH 7.5, 1 mmol/L DTT) were loaded with GTP and protein concentration adjusted to 2 mg/mL. The assay was performed in a clear 384-well plate (Costar) by mixing 50 μ L of protein (50 μ mol/L final concentration), 20 μ L of MESH (200 μ mol/L), and 5 μ L of purine nucleotide phosphorylase (0.5 U). GTP hydrolysis was initiated by the addition of either 25 μ L of assay buffer with 40 mmol/L MgCl₂ (intrinsic) or 25 μ L (50 μ mol/L final concentration) of P120GAP (GAP stimulated). The absorbance at 360 nm was read every 8 to 15 seconds for 1,000 seconds at 20°C.

RAF kinase interaction assay

KRAS:RAF kinase interaction assays were performed as previously described (35). Purified RAF kinase RBD was labeled with maleimide PEG biotin (Pierce) following the manufacturer's recommended protocol. Purified flag-tagged KRAS (1 mg/mL) and KRAS mutants were loaded with GMPPNP (Sigma-Aldrich) by incubating for 2 hours at 25°C with a 50-fold excess of nucleotide in the presence of alkaline phosphatase (Thermo-Fisher). RAF-RBD-biotin was diluted to a final concentration of 40 nmol/L and Flag-KRAS to 10 nmol/L in assay buffer (20 mmol/L Tris pH 7.5, 100 mmol/L NaCl, 1 mmol/L MgCl₂, 5% glycerol, 0.5% BSA) and added to individual wells of a low-volume white 384-well plate (PerkinElmer). Complexes were disrupted by addition of a dilution series (2,000 nmol/L to 0.5 nmol/L) of each mutant KRAS protein. The assay was developed by addition of streptavidin donor and anti-flag acceptor AlphaScreen beads (10 μ g/mL). Alpha signal was measured after overnight incubation at 4°C.

KRAS X-ray crystal structure determination

Crystals of KRAS mutants grew from hanging vapor diffusion drops with various solutions in the reservoir: 0.2 mol/L sodium acetate pH 4.5, 0.1 mol/L Tris pH 8.5, 28% PEG 3,350 (G12R), 0.2 mol/L sodium acetate pH 4.5, 0.1 mol/L Tris pH 8.5, 24% PEG 3,350 (G12V), 0.2 mol/L sodium acetate pH 4.5, 0.1 mol/L Tris pH 8.5, 26% PEG 3,350 (G13D, Q61L), 0.1 mol/L MMT pH 4.0, 24% PEG 6000. Crystals were cryoprotected in 15% glycerol and flash-frozen in liquid nitrogen. Diffraction images were collected at the advanced photon source beamline 19-ID. Data were integrated and scaled using HKL2000/3000 packages (36). Molecular replacement was performed with 4OBE as the search model using Phaser software. Manual and automated model building and refinement were performed using Phenix package and coot software (37, 38). Figure images were prepared using Pymol (The PyMOL Molecular Graphics System, Version 1.5.0.4 Schrödinger, LLC). Final model and scaled reflection data were deposited at the Protein Data Bank. Final collection and refinement statistics are presented in Supplementary Table S1.

Electrostatic maps of wild-type (WT) KRAS (PDB ID 4OBE) and KRAS G13D were generated using the PDB2PQR server (39, 40) with the PARSE force field and PROPKA to assign protonation states. Images were prepared using the Pymol APBS tools plugin (41). Modeling of KRAS G12R bound to RAF kinase was done by aligning the G12R structure onto the structure of HRAS bound to the RBD of RAF kinase (PDB ID 4G0N) using Pymol software.

CCLE data analysis

We downloaded pharmacologic profiles for 24 compounds tested against 504 cell lines from the CCLE database (42) and analyzed the results of cell lines treated with two different MEK inhibitors, AZD6244, PD-0325901, and two RAF inhibitors, PLX4720, and RAF265. We categorized each based on KRAS status, WT or mutant after removing from this analysis any cell lines that harbored mutations in BRAF, HRAS, NRAS, EGFR, PI3K, or PTEN. We then calculated the mean reported IC₅₀ for each group, WT vs. mutant KRAS, to determine the effect of KRAS mutations on sensitivity to MEK inhibition. Of the four compounds, only one, PD-0325901, had a significantly lower IC for mutant KRAS cell lines compared with WT KRAS. For this compound, we further stratified the cell lines into specific KRAS mutations and plotted mean IC₅₀ values for each.

Results

KRAS-mutant nucleotide kinetics

Direct targeting of the RAS GTP-binding site has been dismissed as a therapeutic strategy in large measure because RAS has a high affinity for GTP and GDP nucleotides with dissociation constants in the picomolar range (43–45). However, the nucleotide-binding characteristics of specific oncogenic KRAS isoforms have not been systematically examined. The commonly observed oncogenic mutations at positions 12, 13, and 61 cluster around the nucleotide-binding site, raising the possibility that certain mutations may destabilize interactions between RAS and GTP or GDP or provide other opportunities to target RAS. Indeed, we recently reported that the active site of KRAS G12C can be targeted by small molecules bearing an electrophilic warhead that covalently binds to the mutant cysteine in position 12 (34, 35). Ostrem and colleagues (46) also exploited this mutation to develop covalent inhibitors that target a pocket adjacent to the active site, but found that these inhibitors preferentially bind to the GDP-bound form and therefore, depend in some measure on nucleotide exchange or hydrolysis. In addition, it is possible that nucleotide exchange may influence the signaling behaviors of specific mutant RAS isoforms. We therefore surveyed the kinetics of nucleotide exchange for nine of the most common KRAS isoforms.

We adapted from previously reported methods that use a fluorescently labeled GDP and GTP analogues (45), to measure the nucleotide exchange kinetics of KRAS mutants. The binding assay takes advantage of a shift in the fluorescence emission from 441 to 432 nm and change in fluorescence intensity when mant-labeled nucleotides are RAS-bound. This allows monitoring of nucleotide dissociation in real-time (46–48). Kinetics of nucleotide exchange were essentially identical between mutants and WT, with the exception of G13D, which has a GDP exchange rate 14 times faster than WT (0.027/s vs. 0.002/s) and a GTP exchange rate nine times faster than WT (0.018/s vs. 0.002/s; Fig. 1).

Intrinsic KRAS-mutant GTPase activity

KRAS has an intrinsic GTPase activity that allows the enzyme to auto-inactivate signal propagation. To determine the effect of oncogenic mutations on the intrinsic GTP hydrolysis rate, we used a purine nucleoside phosphorylase-based (PNP) assay to measure phosphate release in real-time (49). In our assay, the intrinsic hydrolysis rate of WT KRAS is slow, 68×10^{-5} /s, comparable with previously reported rates for RAS (44, 50, 51).

Hunter et al.

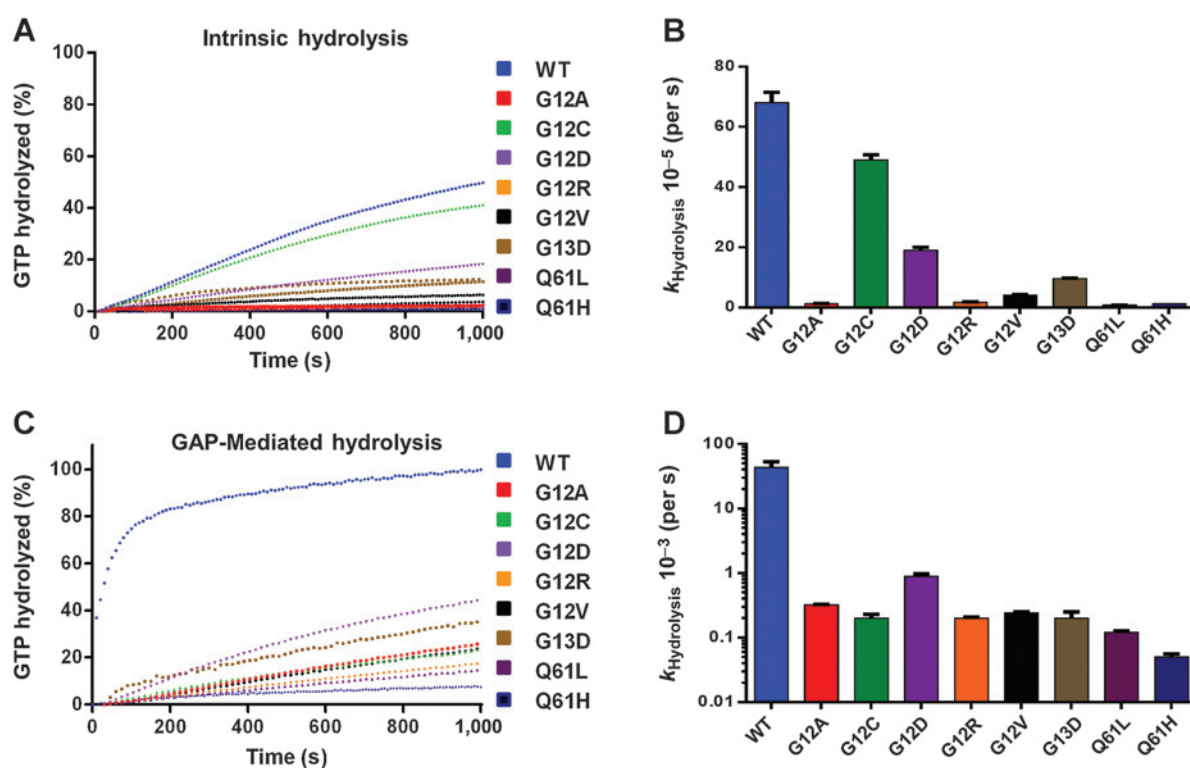


Figure 2.

GTPase kinetics. WT and mutant KRAS proteins were loaded with GTP and the rate of intrinsic GTP hydrolysis (A and B) or GAP stimulated GTP hydrolysis (C and D) was determined by continuously measuring phosphate using a purine nucleoside phosphorylase-based colorimetric assay. The concentration of phosphate released vs. time was plotted and the first-order rate constant determined. Data are the mean of three replicates \pm standard error.

Intrinsic hydrolysis rates for each of the mutants were highly variable. The G12C mutation had minimal impact on the intrinsic hydrolysis rate while mutation of G12 to A or R and mutation of Q61 to H or L lead to an approximately 40- to 80-fold decrease in GTP hydrolysis rate. G12 to D and V and G13 to D had an intermediate effect (Fig. 2A and B and Table 1).

GAP-stimulated KRAS-mutant GTPase activity

Mutations in codons 12 and 13 dampen RAS responses to GAPs, such as P120GAP and NF1, resulting in slower rates of stimulated GTP hydrolysis (27, 52). Extrapolation from structural studies suggests that these mutations cause a steric clash with a catalytic arginine residue (also known as the "arginine finger") that is donated by GAPs, preventing access to the nucleotide binding domain (53). This insensitivity to GAP regulation leads

to prolonged RAS activation and propagation of progrowth signaling. We wondered whether differences in sensitivity to GAP stimulation between position 12, 13, and 61 mutants, *en masse* within the cell, might account for some of the observed clinical mutation-specific differences. We therefore measured the rate of GTP hydrolysis for each of the mutants in response to P120GAP stimulation, using the PNP assay. As expected, we saw a dose-dependent increase in the observed rate of phosphate release from WT KRAS with addition of P120GAP (Supplementary Fig. S1). However, due to the speed limitations of our assay setup, we were unable to accurately measure the rapid hydrolysis rate of WT KRAS at saturating concentrations of P120GAP. We therefore profiled each of the mutant forms of KRAS at a subsaturating concentration, 50 $\mu\text{mol/L}$ P120GAP, to obtain relative GAP-stimulated hydrolysis measurements. Each of the KRAS mutants exhibited a significant, 97% to 99% decrease in the rate of GAP-stimulated hydrolysis compared with WT KRAS (Fig. 2C and D). However, some of the KRAS mutants appeared to be more responsive to GAP-mediated stimulation in the rate of GTP hydrolysis than others. In particular, the GAP-stimulated rate for Q61L and G12A is approximately 15- to 25-fold higher than their intrinsic rates, suggesting that a portion of the GAP-dependent catalytic mechanism is still somewhat functional in these mutants (Table 1).

KRAS-mutant affinities for RAF RBD

KRAS propagates signals through direct interactions with downstream effectors that generally bind to RAS in the regions

Table 1. Intrinsic and GAP-stimulated GTP hydrolysis rates

| | $k_{\text{hydrolysis}} \cdot 10^{-5} \text{ (sec}^{-1}\text{)}$ | | |
|------|---|------------|--------------------|
| | Intrinsic | | P120GAP Stimulated |
| WT | 68 | ± 3.5 | 4,300 ± 100 |
| G12A | 1.3 | ± 0.06 | 32 ± 0.8 |
| G12C | 49 | ± 1.8 | 20 ± 3 |
| G12D | 19 | ± 1 | 89 ± 8 |
| G12R | 1.8 | ± 0.07 | 20 ± 0.8 |
| G12V | 4.2 | ± 0.2 | 24 ± 1 |
| G13D | 9.6 | ± 0.2 | 20 ± 5 |
| Q61L | 0.80 | ± 0.05 | 12 ± 0.7 |
| Q61H | 1.3 | ± 0.03 | 5 ± 0.6 |

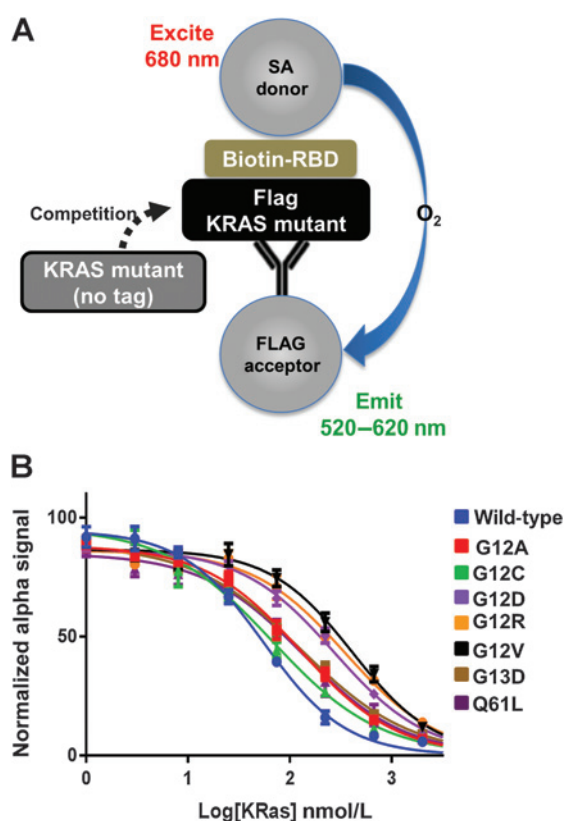


Figure 3. Relative affinity of RAF kinase for KRAS mutants. A, schematic of assay principle. In the competitive AlphaScreen bead-based assay, untagged KRAS protein is used to compete apart preformed complexes of KRAS with the RBD of RAF kinase. B, dilution series of untagged KRAS mutants disrupted RAS-RAF RBD complexes leading to loss of alpha signal. Data, mean of three separate experiments \pm SE.

around switches 1 and 2 (30, 31, 54). Codon 61 is in switch 2 and therefore could be expected to perturb interactions with effectors. Codons 12 and 13 are found within the P-loop of the enzyme, near the β and γ phosphates of GTP and directly adjacent to the switches and could also directly affect changes on the switch conformation (34). We therefore anticipated that mutations at positions 12, 13, or 61 would decrease the affinity of KRAS for effectors that interact with the switch interface. RAF kinase is directly downstream of KRAS in the MAPK pathway and is activated through a direct interaction with the switch 1 domain of KRAS. We previously developed a sensitive AlphaScreen-based competition assay to measure the effects of the GTP-competitive inhibitor SML-8-73-1 on KRAS G12C interactions with the RBD of RAF kinase (34, 35). Here, we adapted this to measure the relative affinity of the various KRAS mutants for RAF-RBD (Fig. 3A). Mutations at all three positions result in a significant and variable decrease in affinity. Mutations at positions 13 and 61 as well as G12 to A or C show only a small, 1.2- to 2.3-fold decrease in relative affinity compared with WT KRAS. In contrast, substitution of bulkier side chains, including D, V, or R, at position 12 lead to a more significant 4.8-, 7.3-, and 6.2-fold decrease in affinity, respectively (Fig. 3B and Table 2).

Table 2. Relative affinities for RAF kinase

| Relative RAF kinase affinity (nmol/L) | | |
|---------------------------------------|-----|----------|
| WT | 56 | ± 6 |
| G12A | 127 | ± 12 |
| G12C | 67 | ± 12 |
| G12D | 270 | ± 46 |
| G12R | 348 | ± 29 |
| G12V | 411 | ± 40 |
| G13D | 129 | ± 15 |
| Q61L | 134 | ± 26 |

X-ray structures of mutant KRAS

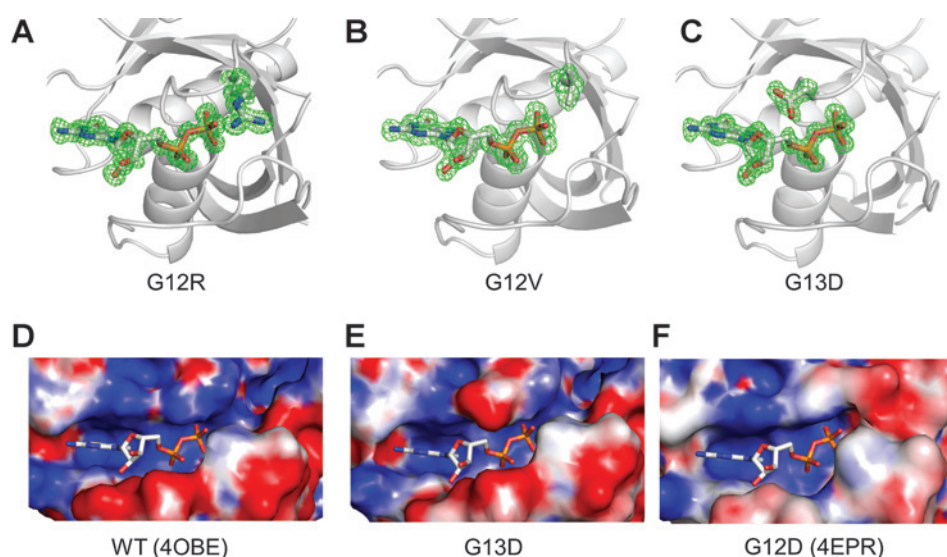
Numerous structures of HRAS and KRAS have now been solved. KRAS G12C, in particular, has been the subject of efforts to directly target that specific oncogenic KRAS subtype and numerous structures were solved as part of that effort (34, 46). To further understand the effect of other common KRAS mutations on the protein structure and perhaps explain some of the observed differences in biochemical properties we solved high-resolution X-ray structures of four KRAS mutants in complex with GDP, including G12V, G12R, G13D, and Q61L. Crystals grew from previously reported hanging drop conditions in C2, P212121, and P63 space groups. X-ray diffraction ranged from 1.0 to 2.0 Å as detailed in Supplementary Table S1. Phases were determined from molecular replacement using 4OBE as the search model and the structures were further refined using the Phenix software package.

Mutations have a minimal effect on the overall structure of the protein with global RMSDs of 0.115, 0.351, 0.146, and 0.677 Å for G12V, G12R, G13D, and Q61L, respectively, compared with WT KRAS. The switch 1 and switch 2 regions for all four mutants are in the open conformation very similar to the WT and G12C structures we reported previously (34). The structure of Q61L mutant form of KRAS showed good density for all regions of the protein except for residues 60 to 70 (including L61) on switch 2 that were disordered and the density was insufficient to build this region into our model. This was the only mutant to crystallize in the P63 space group and crystal contacts appear to contribute to the disorder in this region.

For the G12 and G13 mutants, we observed strong *fo*-*fc* density corresponding to the side chain atoms of valine, arginine, aspartate in the respective structures and we modeled the residues into this density (Fig. 4A-C). The side chains of G12V and G12R extend from the P-loop directly over the γ -phosphate binding pocket similar to the cysteine side chain of G12C KRAS. The guanidinium group of R12 and the branched chain carbon atoms of V12 are within van der Waals distance (3.5 and 3.9 Å, respectively) of P34 in switch 1, occluding the terminal phosphates from the solvent. Indeed, in the G12R structure, we observe that an ordered water molecule, which was observed to coordinate with the β -phosphate of GDP in the WT structure, is displaced by the arginine mutation.

In KRAS G13D, the aspartate side chain is positioned above the α -phosphate and rotated with the carboxyl group pointing toward the ribose ring of GDP with the carboxylic oxygen atoms sitting approximately 3 Å from carbon-5 of the ribose sugar group. In WT KRAS, the P-loop region above the phosphate groups is strongly positive, facilitating binding of the negatively charged phosphates. However, substitution of aspartate at position 13 perturbs the local electrostatic environment of the phosphate-binding pocket, introducing a significant

Hunter et al.

**Figure 4.**

Crystal structures of KRAS mutants. A–C, the X-ray crystal structure of four KRAS mutants, G12R (A), G12V (B), and G13D (C) were solved. Q61L is not shown because switch 2 is disordered because of crystal contacts. Position 12 and 13 side chain atoms and nucleotide were modeled into the continuous *fo–fc* positive density (green). D and E, electrostatic potential maps were calculated using the PDB2PQR server and APBS tools for both WT (D) and G13D (E) KRAS and show disruption of the positive (blue) charge above the alpha phosphate of the nucleotide in the presence of the G13D mutation. F, the structure of KRAS G12D is shown for comparison demonstrating that the 12D substitution does not disrupt the charge distribution surrounding the α and β phosphates.

negative charge in this region. In contrast, an electrostatic map of G12D KRAS calculated from the published structure (PDB ID: 4EPR) demonstrates much less disruption of the positively charged binding pocket (Fig. 4D–F; ref. 55).

Discussion

Nucleotide binding

Within the cell, nucleotide exchange is modulated by GEFs such as SOS. Upon KRAS binding to a GEF, the nucleotide-binding cleft is pried open causing KRAS to release its bound nucleotide and allowing KRAS to become GTP bound and, therefore, activated for signaling (28). GTP (as opposed to GDP) binding is thought to be driven by the high concentration of GTP within the cell, 5- to 10-fold higher than GDP, as well as the higher-affinity WT KRAS has for GTP over GDP rather than any active preferential loading of GTP by GEFs (28, 56). We found that the rate of SOS-independent nucleotide exchange for KRAS G13D is an order of magnitude faster than WT KRAS, suggesting that this mutant may be able to more frequently auto-activate by spontaneously exchanging GDP for GTP. This finding is consistent with molecular dynamic simulations (57) and is likely explained structurally by the change in the electrostatic environment around the nucleotide and increased repulsion between the negatively charged carboxylic group of D13 and the α -phosphate group. Increased auto-activation would make KRAS G13D less dependent on GEF regulation, leading to increased aberrant RAS signaling in these cells. A previous report looking at exchange kinetics for G13D HRAS using NMR also found a similar approximately 15-fold increase in nucleotide exchange rate for G13D compared with WT HRAS, indicating that SOS-independent auto-activation may be a general phenomenon for all G13D mutants of RAS-family members (58). The relatively fast exchange kinetics measured for the G13D mutant could contribute to the more aggressive biology of G13D-associated tumors seen in some studies (59), although there are also contexts in which G13D-associated tumors interact favorably with specific treatment regimens (26). We also note that the fast exchange kinetics of G13D may provide more access to the active site for small-molecule

inhibitors if compounds with sufficient binding affinity can be developed.

GTP hydrolysis

Although many studies suggest that GAP-stimulated hydrolysis rates predominate over intrinsic hydrolysis and therefore have the most significant impact on biology, and this certainly seems to be the case for WT, the marked GAP insensitivity we see with the mutants raises the possibility that intrinsic rates may play a significant role in regulating the duration of mutant KRAS signaling. Because the affinity between WT KRAS and GAPs is low (~ 0.1 – $1 \mu\text{mol/L}$ *in vitro*) and the complex has a relatively rapid dissociation rate ($\sim 7.5/\text{s}$) the life of the complex is likely shorter than the rate of hydrolysis (60). Effectively this suggests that for many oncogenic KRAS mutants, intrinsic GTP hydrolysis may be the dominant process responsible for inactivation of RAS signaling through all of its downstream effectors. The corollary to this concept is that differences in intrinsic hydrolysis rates between the mutants may translate into different biologic behaviors.

Even for WT KRAS, it has been proposed that RAS signaling through the RAF kinase pathway is regulated primarily through RAS's intrinsic GTP hydrolysis rather than GAP-dependent hydrolysis (61). This reasoning is based on the observation that the affinity between KRAS and RAF kinase is in the low nanomolar range, approximately 10 to 50 nmol/L, whereas the dissociation constants for KRAS and its other main effectors, including PI3K and RalGDS, is in the low micromolar range (30, 62). Because the predominant GAPs that regulate KRAS signaling, P120GAP and NF1, also have affinities in the low micromolar range and bind to overlapping regions of the protein, it has been proposed that GAPs are unable to effectively compete against RAF kinase to accelerate GTP hydrolysis and therefore RAS signaling through the RAF pathway is deactivated solely through its intrinsic GTPase activity (63, 64).

A precise structural explanation for the mechanistic differences in intrinsic GTP hydrolysis rates for different mutants will likely be incomplete until a structure of mutant RAS in the GTP hydrolysis transition state is available. However, predictions about general processes can be inferred from the available

structures of H and KRAS, the structure of P120GAP in complex with HRAS, and relevant biochemical measurements (52). The structure of HRAS bound to a transition state analogue, GDP- AlF_3 , in complex with P120GAP demonstrates that during hydrolysis Q61 coordinates a nucleophilic water molecule near the γ -phosphate of GTP (Supplementary Fig. S2; ref. 65). This coordination is also likely a critical component of intrinsic GTP hydrolysis as evidenced by the fact that the Q61L and Q61H mutants exhibit the lowest intrinsic GTP hydrolysis rates (64). Notably, structures of a closely related small GTPase, RAB5a, bound to GTP or the transition state analogue GDP- AlF_3 show that the equivalent glutamine residue moves to this coordinated position during the transition state even for the intrinsic GTP hydrolysis reaction (PDBIDs: 1N6L and 1N6K). For KRAS therefore, it is likely that in GAP-independent GTP hydrolysis the flexibility of Q61 in solution allows it to transiently adopt the coordinated conformation allowing GTP hydrolysis to occur. There has also been some suggestion that coordination of Q61 during intrinsic hydrolysis may in fact be regulated allosterically, but the identity of the endogenous modulator has yet to be determined (64). Together, these observations add to prior evidence pointing to the critical role of Q61 in GTP hydrolysis.

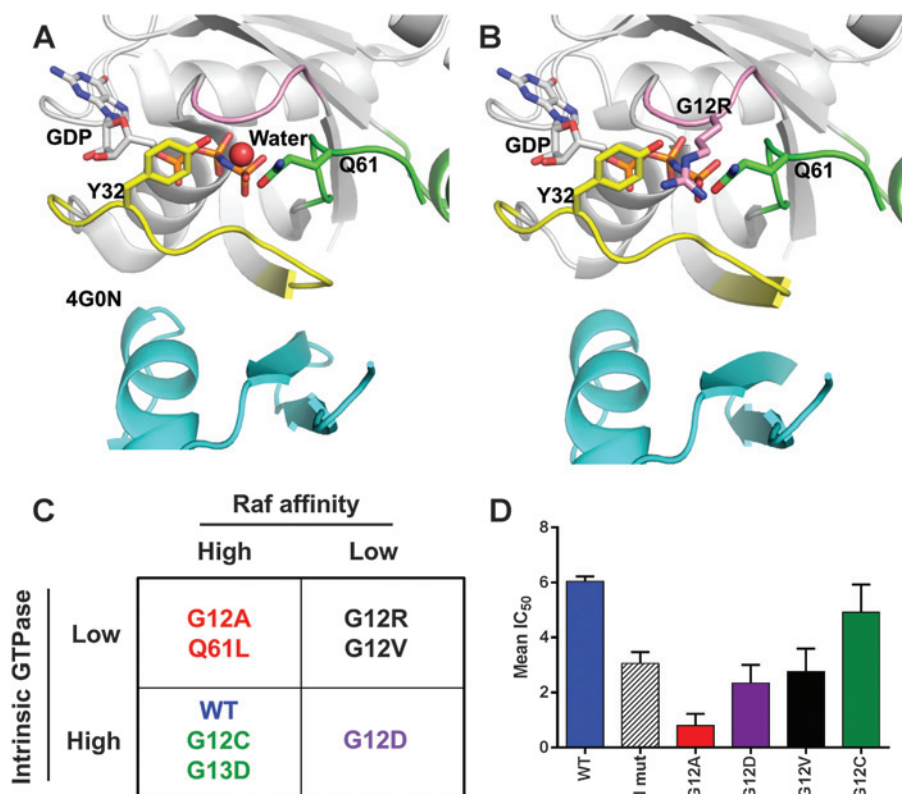
In contrast, the structural explanation for the significant decrease in the rate of intrinsic GTP hydrolysis observed for position 12 and 13 mutants is less clear. At a high level, a rendering of WT KRAS using an electrostatic potential map shows that the phosphate binding pocket is strongly positively charged, likely allowing stabilization of negative charge on the phosphates

(Fig. 4D). This general feature likely contributes to a complex dissociative process in which RAS catalyzes hydrolysis, in part, by distributing accumulating negative charges on the β -phosphate. The backbone nitrogen atoms of G12 and G13 are within hydrogen bonding distance of the β -phosphate of GDP and GTP and significantly contribute to the overall charge stabilization during hydrolysis. Although our structures show that positioning of the P-loop main chain nitrogen atoms are unaffected by any of the G12 and G13 mutations, mutations in this region can have significant effects on the local electrostatic environment as demonstrated in Fig. 4 and likely affect the transition state energy landscape. To further probe what effect position 12 mutants may have on the catalysis, we generated a model of KRAS G12R in the GTP hydrolysis transition state by aligning our KRAS G12R structures with the published structure of HRAS bound to P120GAP in the transition state (PDB ID: 1WQ1). In this model, the side chain atoms of R12 sit approximately 1.7\AA from N61, well within van der Waals distance (Supplementary Fig. S2). This clash may limit the flexibility of Q61 and its ability to coordinate the nucleophilic water, destabilizing the transition state.

It has also been proposed that Y32 on switch I plays an important role in intrinsic hydrolysis by coordinating a water molecule adjacent to the β -phosphate, allowing it to stabilize accumulating negative charges in a manner similar to the arginine finger of GAPs (64). Modeling bulky position 12 mutants, such as R12, onto the structure of activated RAS in complex with RAF kinase demonstrate a clash with Y32 and displacement of the adjacent coordinated water, suggesting an additional mechanism of disrupting intrinsic hydrolysis (Fig. 5A and B). In contrast,

Figure 5.

Predicted impact of KRAS mutations on RAF kinase signaling. A, published structure of HRAS (white) in complex with the RBD of RAF kinase (cyan, PDB ID: 4G0N). In the complex switch I (yellow) and switch II (green) are in the closed conformation and Y32 and Q61 rotate toward the γ phosphate of GMPPNP. B, model of G12R KRAS bound to the RBD of RAF kinase prepared by aligning the G12R-mutant structure to A. In this model, the P-loop (pink) R12 side chain atoms clash with both Q61 and Y32 residues and displaces a coordinated solvent molecule. These predicted perturbations may lead to some destabilization of both switch I (yellow) and switch II (green) regions and a perhaps explain the decrease in affinity observed for G12R KRAS. C, proposed classification scheme of KRAS mutants based on intrinsic GTP hydrolysis rates and relative affinity for RAF kinase. D, KRAS-mutant cell lines show differential sensitivity to the MEK inhibitor PD-0325901. Publicly available sequencing and pharmacologic data from the cancer cell line encyclopedia were downloaded from the Broad institute and mean IC_{50} values for each KRAS mutant calculated \pm SE.



Hunter et al.

modeling G13D onto the activated KRAS structure demonstrates that the side chain atoms of D13 are approximately 4 Å from Y32 and face the opposite side of the P-loop and would not be predicted to have an impact on Q61 positioning. Therefore, it seems likely that the approximately 7-fold decrease in hydrolysis rate observed for G13D is due to the change in the regional electrostatics characterized by a decrease in the overall positive charge of the phosphate binding pocket and perhaps a decreased ability to stabilize the developing negative charge on the β -phosphate (Fig. 4D and E).

In the case of position 12 mutations that introduce smaller amino acids, additional processes are likely involved. Notably, G12C exhibits an intrinsic GTP hydrolysis rate almost equivalent to WT KRAS while G12A, the position 12 mutant with the smallest side chain, has one of the slowest rates. Electrostatic arguments again may help explain these effects. Insertion of alanine, a nonpolar amino acid, directly above the γ -phosphate of GTP may alter the charge distribution or cause some reordering of the solvent, and account for the slow hydrolysis rates. In contrast, cysteine, a polar amino acid, may improve the local environment and therefore have less of an overall impact on the intrinsic hydrolysis rate. In the crystal structure of HRAS G12C bound to GMPPNP (PDB ID 4L9W), one conformation of the cysteine side chain shows the sulfur atom involved in a hydrogen bonding network with the Y32 coordinated water molecule adjacent to the phosphate. This additional coordination may account for its near WT rate of intrinsic hydrolysis.

KRAS interaction with RAF

We observed that mutations that substitute bulky side chains at position 12 result in a significant decrease in the affinity of KRAS for RAF kinase. Because the RBD of RAF kinase interacts with the distal face of switch I relative to the nucleotide binding pocket, approximately 12 Å from G12 we wanted to understand how mutations at this position could have a significant impact on the affinity of KRAS for RAF-RBD. To do this, we aligned our structures of KRAS R12 and V12 onto the structure of the complex between HRAS and the RBD of RAF-kinase (Fig. 5A and B, PDB ID 4G0N). When bound to RAF, switch 1 assumes a closed conformation with Y32 rotated up pointing toward the P-loop. Our model demonstrated that when mutated to V or R the side chain carbon atoms are between 2.3 and 2.6 Å from the oxygen atom in the side chain of Y32, within van der Waals distance. On the basis of this, we propose that in these mutants, Y32 may be shifted outward causing a slight reordering of switch 1 leading to a concomitant decrease in affinity with RBD.

Correlations with biologic data

Our overarching goal is to establish a biochemical basis for sorting specific KRAS mutations into biologic subclasses that inform future laboratory-based or clinical studies. An attractive approach is to attempt to group mutations by which signaling pathways may be preferentially activated by specific KRAS mutations. This would provide biologic selection criteria for experiments or clinical trials that include agents that target one pathway or another (MAPK vs. PI3K/AKT, for example). Such a scheme would also provide a set of testable hypotheses about the differential impact each of the various KRAS mutations has on RAS signaling pathways.

One possible interpretation of the combined KRAS:RAF interaction and intrinsic hydrolysis data is that KRAS muta-

tions with a high RAF affinity and low intrinsic GTPase rate will exhibit increased and sustained RAF activation compared with KRAS mutants with a low RAF affinity and more rapid intrinsic hydrolysis. With this as a standard, we can broadly classify the different mutant forms of KRAS into the following categories: those with a high (WT, G12C, G12D, G13D) and low (G12A, G12R, G12V, Q61L, and Q61H) level of intrinsic GTPase activity. We can further classify the mutants as high RAF affinity (WT, G12A, G12C, G13D, and Q61L) or low RAF affinity (G12R, G12V, and G12D) based on their relative affinity for RAF kinase RBD. Combining these criteria, we arrive at a hypothetical scheme for predicting the relative dependence on or activation of the RAF kinase pathway compared with other pathways, such as PI3K or RalGDS, in tumors harboring specific KRAS mutations. The scheme presented in Fig. 5C predicts that G12A- and Q61L-bearing tumors preferentially signal through the RAF kinase pathway due to their high affinity for RAF kinase and relatively lower rates of intrinsic hydrolysis. In contrast, G12D with its low affinity for RAF and faster hydrolysis rate would be predicted to show the lowest levels of RAF activation. The model further predicts that G12V and G12R would show moderate activation of RAF kinase due to their slow intrinsic hydrolysis rate coupled with a low RAF affinity. Likewise, G12C and G13D would be predicted to moderately activate RAF kinase due to their high affinity, but because they have a more rapid intrinsic GTPase activity, the duration of the activation is likely attenuated compared with G12A and Q61.

It is intriguing that this classification is compatible with other lines of previously reported data, both in animal models and human tumors. For example, Buhrman and colleagues (61) reported that cells expressing KRAS Q61L had significantly higher levels of RAF-dependent MEK phosphorylation than did cells expressing KRAS G12V. The authors propose that this effect is due to the differences in the intrinsic hydrolysis rate, but our results would indicate that a second factor, the relative affinity of the mutants for RAF kinase may also contribute. We also note that Q61L mutations occur proportionately more frequently in tumors that also show a high rate of BRAF mutations, suggesting that this pathway is favored by Q61L mutations (66). Cespedes and colleagues demonstrated that while ectopically expressed KRAS G12D, predicted to be a low RAF activator, associates with PI3K, it does not associate with RAF kinase nor lead to ERK phosphorylation in NIH3T3 cells. In contrast, KRAS G12V, predicted to be a moderate RAF activator in our study, associated with both RAF kinase and PI3K in these cells (67). Ihle and colleagues (19) observed that a KRAS G12D expressing non-small cell lung cancer cell line exhibited a significant increase in growth factor-independent activation of PI3K signaling compared with KRAS G12C or KRAS WT expressing NSCLC cells, perhaps indicating that with a decreased affinity for RAF kinase, KRAS G12D preferentially signals through PI3K, at least in some cell lines. This proposed classification scheme obviously does not take into account the many other relevant parameters of KRAS biology, including GEF-stimulated and intrinsic nucleotide exchange, affinity for other downstream effectors, including PI3K and RalGDS. However, it does begin to suggest the various axes along which we may stratify KRAS mutants toward a complete understanding of their oncogenic behavior.

As a high-level test of this initial biochemical categorization, we attempted to correlate with data from the Broad Institute cancer cell line encyclopedia (CCLE; ref. 42). This database contains drug sensitivity data for a large number of tumor cell lines against 24 different cytotoxic agents, of which 4 were predicted to be active against the MAPK pathway. Each of these cell lines was further analyzed by exome and genomic SNP sequencing to determine the mutation status of approximately 1,650 genes. In total, 85 of 365 cell lines had KRAS mutations, including G12A ($n = 3$), G12C ($n = 15$), G12D ($n = 27$), G12R ($n = 4$), G12S ($n = 2$), G12V ($n = 19$), G13C ($n = 3$), G13D ($n = 7$), and Q61 ($n = 5$) alterations. Tumors with KRAS mutations were generally insensitive to three of the inhibitors but did show differential sensitivity to the MEK inhibitor PD-0325901. Mean sensitivity (IC_{50}) to PD-0325901 is plotted in Fig. 5D and, interestingly, correspond to our classification scheme with cell lines bearing mutations predicted to be most dependent on RAF signaling, such as KRAS G12A, having the lowest IC_{50} s for PD-0325901. G12D, G12V, G12C, or WT KRAS cells were less sensitive, whereas G12C-bearing cell lines had about the same level of sensitivity as cells bearing WT KRAS, which in our model would be attributed to similar hydrolysis rates and RAF affinities between KRAS G12C and WT. Clearly these studies are only hypothesis generating and require additional validation, but raise the interesting possibility that specific KRAS mutations could be used as selection criteria for targeted therapies against specific pathways downstream of KRAS.

Disclosure of Potential Conflicts of Interest

No potential conflicts of interest were disclosed.

References

- Parada LF, Tabin CJ, Shih C, Weinberg RA. Human EJ bladder carcinoma oncogene is homologue of Harvey sarcoma virus ras gene. *Nature* 1982; 297:474–8.
- Der CJ, Krontiris TG, Cooper GM. Transforming genes of human bladder and lung carcinoma cell lines are homologous to the ras genes of Harvey and Kirsten sarcoma viruses. *Proc Natl Acad Sci U S A* 1982; 79:3637–40.
- Eberhard DA, Johnson BE, Amler LC, Goddard AD, Heldens SL, Herbst RS, et al. Mutations in the epidermal growth factor receptor and in KRAS are predictive and prognostic indicators in patients with non-small-cell lung cancer treated with chemotherapy alone and in combination with erlotinib. *J Clin Oncol* 2005;23: 5900–9.
- Forbes SA, Bhamra G, Bamford S, Dawson E, Kok C, Clements J, et al. The Catalogue of Somatic Mutations in Cancer (COSMIC). *Curr Protoc Hum Genet* 2008;Chapter 10:Unit 10.1.
- Prior IA, Lewis PD, Mattos C. A comprehensive survey of Ras mutations in cancer. *Cancer Res* 2012;72:2457–67.
- Society AC. Cancer facts & figures 2013. [cited October 1, 2014]. Available from: <http://www.cancer.org/acs/groups/content/@epidemiologysurveillance/documents/document/acspc-036845.pdf>.
- Seeburg PH, Colby WW, Capon DJ, Goeddel DV, Levinson AD. Biological properties of human c-Ha-ras1 genes mutated at codon 12. *Nature* 1984;312:71–5.
- Der CJ, Finkel T, Cooper GM. Biological and biochemical properties of human rasH genes mutated at codon 61. *Cell* 1986;44:167–76.
- Cox AD, Fesik SW, Kimmelman AC, Luo J, Der CJ. Drugging the undruggable RAS: mission Possible? *Nat Rev Drug Discov* 2014;13: 828–51.
- Stephen AG, Esposito D, Bagni RK, McCormick F. Dragging ras back in the ring. *Cancer Cell* 2014;25:272–81.
- Forbes SA, Bindal N, Bamford S, Cole C, Kok CY, Beare D, et al. COSMIC: mining complete cancer genomes in the Catalogue of Somatic Mutations in Cancer. *Nucleic Acids Res* 2011;39:D945–50.
- Zarbl H, Sukumar S, Arthur AV, Martin-Zanca D, Barbacid M. Direct mutagenesis of Ha-ras-1 oncogenes by N-nitroso-N-methylurea during initiation of mammary carcinogenesis in rats. *Nature* 1985;315: 382–5.
- Törmänen V, Pfeifer G. Mapping of UV photoproducts within ras proto-oncogenes in UV-irradiated cells: correlation with mutations in human skin cancer. *Oncogene* 1992;7:1729–36.
- Gougopoulou DM, Kiaris H, Ergazaki M, Agnostonopoulos NI, Grigoraki V, Spandidos DA. Mutations and expression of the ras family genes in leukemias. *Stem Cells* 1996;14:725–9.
- Denissenko MF, Pao A, Pfeifer GP, Tang M-s. Slow repair of bulky DNA adducts along the nontranscribed strand of the human p53 gene may explain the strand bias of transversion mutations in cancers. *Oncogene* 1998;16:1241–7.
- Lampson BL, Pershing NL, Prinz JA, Lacsina JR, Marzluff WF, Nicchitta CV, et al. Rare codons regulate KRas oncogenesis. *Curr Biol* 2013;23: 70–5.
- Sarkisian CJ, Keister BA, Stairs DB, Boxer RB, Moody SE, Chodosh LA. Dose-dependent oncogene-induced senescence *in vivo* and its evasion during mammary tumorigenesis. *Nat Cell Biol* 2007;9: 493–505.
- Westcott PM, Halliwill KD, To MD, Rashid M, Rust AG, Keane TM, et al. The mutational landscapes of genetic and chemical models of Kras-driven lung cancer. *Nature* 2015;517:489–92.

Authors' Contributions

Conception and design: J.C. Hunter, A. Manandhar, M.A. Carrasco, K.D. Westover
Development of methodology: J.C. Hunter, A. Manandhar, M.A. Carrasco, D. Gurbani, K.D. Westover

Acquisition of data (provided animals, acquired and managed patients, provided facilities, etc.): J.C. Hunter, A. Manandhar, M.A. Carrasco, D. Gurbani, K.D. Westover

Analysis and interpretation of data (e.g., statistical analysis, biostatistics, computational analysis): J.C. Hunter, A. Manandhar, M.A. Carrasco, D. Gurbani, S. Gondi, K.D. Westover

Writing, review, and/or revision of the manuscript: J.C. Hunter, M.A. Carrasco, K.D. Westover

Administrative, technical, or material support (i.e., reporting or organizing data, constructing databases): S. Gondi, K.D. Westover

Study supervision: K.D. Westover

Other (lab work, such as PCR, protein expression, protein purification and biochemical studies): S. Gondi

Acknowledgments

Results shown in this article are derived from work performed at Argonne National Laboratory, Structural Biology Center at the Advanced Photon Source. Argonne is operated by U Chicago Argonne, LLC, for the U.S. Department of Energy, Office of Biological and Environmental Research under contract DE-AC02-06CH11357. The authors thank members of the Frederick National Lab for Cancer Research for valuable discussion while preparing the article.

Grant Support

This work was supported by CPRIT (R1207; to K.D. Westover) and The Welch Foundation (11829; to K.D. Westover) and The Pancreatic Cancer Action Network (to J.C. Hunter).

The costs of publication of this article were defrayed in part by the payment of page charges. This article must therefore be hereby marked *advertisement* in accordance with 18 U.S.C. Section 1734 solely to indicate this fact.

Received May 1, 2015; accepted May 20, 2015; published OnlineFirst June 2, 2015.

Hunter et al.

19. Ihle NT, Byers LA, Kim ES, Saintigny P, Lee JJ, Blumenschein GR, et al. Effect of KRAS oncogene substitutions on protein behavior: implications for signaling and clinical outcome. *J Natl Cancer Inst* 2012; 104:228–39.
20. Villaruz LC, Socinski MA, Cunningham DE, Chiosea SI, Burns TF, Siegfried JM, et al. The prognostic and predictive value of KRAS oncogene substitutions in lung adenocarcinoma. *Cancer* 2013;119: 2268–74.
21. Shepherd FA, Domerg C, Hainaut P, Jänne PA, Pignon J-P, Graziano S, et al. Pooled analysis of the prognostic and predictive effects of KRAS mutation status and KRAS mutation subtype in early-stage resected non-small-cell lung cancer in four trials of adjuvant chemotherapy. *J Clin Oncol* 2013; 31:2173–81.
22. Kim ES, Herbst RS, Wistuba II, Lee JJ, Blumenschein GR Jr, Tsao A, et al. The BATTLE trial: personalizing therapy for lung cancer. *Cancer Discov* 2011;1:44–53.
23. Karachaliou N, Mayo C, Costa C, Magri I, Gimenez-Capitan A, Molina-Vila MA, et al. KRAS mutations in lung cancer. *Clin Lung Cancer* 2013; 14:205–14.
24. Garassino MC, Marabese M, Rusconi P, Rulli E, Martelli O, Farina G, et al. Different types of K-Ras mutations could affect drug sensitivity and tumour behaviour in non-small-cell lung cancer. *Ann Oncol* 2011;22: 235–7.
25. Bazan V, Migliavacca M, Zanna I, Tubiolo C, Grassi N, Latteri MA, et al. Specific codon 13 K-ras mutations are predictive of clinical outcome in colorectal cancer patients, whereas codon 12 K-ras mutations are associated with mucinous histotype. *Ann Oncol* 2002;13:1438–46.
26. De Roock W, Jonker DJ, Di Nicolantonio F, Sartore-Bianchi A, Tu D, Siena S, et al. Association of KRAS p.G13D mutation with outcome in patients with chemotherapy-refractory metastatic colorectal cancer treated with cetuximab. *JAMA* 2010;304:1812–20.
27. Gysin S, Salt M, Young A, McCormick F. Therapeutic strategies for targeting ras proteins. *Genes Cancer* 2011;2:359–72.
28. Boriack-Sjodin PA, Margarit SM, Bar-Sagi D, Kuriyan J. The structural basis of the activation of Ras by Sos. *Nature* 1998;394:337–43.
29. Settleman J, Albright CF, Foster LC, Weinberg RA. Association between GTPase activators for Rho and Ras families. *Nature* 1992;359:153–4.
30. Pacold ME, Suire S, Perisic O, Lara-Gonzalez S, Davis CT, Walker EH, et al. Crystal structure and functional analysis of Ras binding to its effector phosphoinositide 3-kinase gamma. *Cell* 2000;103:931–43.
31. Filchtinski D, Sharabi O, Ruppel A, Vetter IR, Herrmann C, Shifman JM. What makes Ras an efficient molecular switch: a computational, biophysical, and structural study of Ras-GDP interactions with mutants of Raf. *J Mol Biol* 2010;399:422–35.
32. Bernardis A, Settleman J. GAP control: regulating the regulators of small GTPases. *Trends Cell Biol* 2004;14:377–85.
33. McCormick F. RAS Pathway v2.0. [cited January 13, 2015]. Available from: <http://www.cancer.gov/research/key-initiatives/ras/ras-central/blog/ras-pathway-v2>.
34. Hunter JC, Gurbani D, Ficarro SB, Carrasco MA, Lim SM, Choi HG, et al. *In situ* selectivity profiling and crystal structure of SML-8-73-1, an active site inhibitor of oncogenic K-Ras G12C. *Proc Natl Acad Sci U S A* 2014;111: 8895–900.
35. Lim SM, Westover KD, Ficarro SB, Harrison RA, Choi HG, Pacold ME, et al. Therapeutic targeting of oncogenic k-ras by a covalent catalytic site inhibitor. *Angew Chem Int Ed Engl* 2014;53:199–204.
36. Minor ZOaW. Processing of X-ray diffraction data collected in oscillation mode. *Methods Enzymol* 1997;276:307–26.
37. Adams PD, Afonine PV, Bunkoczi G, Chen VB, Davis IW, Echols N, et al. PHENIX: a comprehensive Python-based system for macromolecular structure solution. *Acta Crystallogr D Biol Crystallogr* 2010;66:213–21.
38. Emsley P, Lohkamp B, Scott WG, Cowtan K. Features and development of Coot. *Acta Crystallogr D Biol Crystallogr* 2010;66:486–501.
39. Dolinsky TJ, Czodrowski P, Li H, Nielsen JE, Jensen JH, Klebe G, et al. PDB2PQR: expanding and upgrading automated preparation of biomolecular structures for molecular simulations. *Nucleic Acids Res* 2007;35: W522–5.
40. Dolinsky TJ, Nielsen JE, McCammon JA, Baker NA. PDB2PQR: an automated pipeline for the setup of Poisson–Boltzmann electrostatics calculations. *Nucleic Acids Res* 2004;32:W665–7.
41. Baker NA, Sept D, Joseph S, Holst MJ, McCammon JA. Electrostatics of nanosystems: application to microtubules and the ribosome. *Proc Natl Acad Sci U S A* 2001;98:10037–41.
42. Barretina J, Caponigro G, Stransky N, Venkatesan K, Margolin AA, Kim S, et al. The Cancer Cell Line Encyclopedia enables predictive modelling of anticancer drug sensitivity. *Nature* 2012;483:603–7.
43. Feuerstein J, Goody RS, Wittinghofer A. Preparation and characterization of nucleotide-free and metal ion-free p21 "apoprotein." *J Biol Chem* 1987; 262:8455–8.
44. John J, Frech M, Wittinghofer A. Biochemical properties of Ha-ras encoded p21 mutants and mechanism of the autophosphorylation reaction. *J Biol Chem* 1988;263:11792–9.
45. John J, Sohmen R, Feuerstein J, Linke R, Wittinghofer A, Goody RS. Kinetics of interaction of nucleotides with nucleotide-free H-ras p21. *Biochemistry* 1990;29:6058–65.
46. Ostrem JM, Peters U, Sos ML, Wells JA, Shokat KM. K-Ras(G12C) inhibitors allosterically control GTP affinity and effector interactions. *Nature* 2013; 503:548–51.
47. Williams JG, Drugan JK, Yi GS, Clark GJ, Der CJ, Campbell SL. Elucidation of binding determinants and functional consequences of Ras/Raf-cysteine-rich domain interactions. *J Biol Chem* 2000;275: 22172–9.
48. Davis MJ, Ha BH, Holman EC, Halaban R, Schlessinger J, Boggon TJ. RAC1P29S is a spontaneously activating cancer-associated GTPase. *Proc Natl Acad Sci U S A* 2013;110:912–7.
49. Nixon AE, Hunter JL, Bonifacio G, Eccleston JF, Webb MR. Purine nucleoside phosphorylase: its use in a spectroscopic assay for inorganic phosphate and for removing inorganic phosphate with the aid of phospho-deoxyribomutase. *Anal Biochem* 1998;265:299–307.
50. Wey M, Lee J, Jeong SS, Kim J, Heo J. Kinetic mechanisms of mutation-dependent Harvey Ras activation and their relevance for the development of Costello syndrome. *Biochemistry* 2013;52:8465–79.
51. Webb MR, Hunter JL. Interaction of GTPase-activating protein with p21ras, measured using a continuous assay for inorganic phosphate release. *Biochem J* 1992;287(Pt 2):555–9.
52. Scheffzek K, Ahmadian MR, Kabsch W, Wiesmuller L, Lautwein A, Schmitz F, et al. The Ras-RasGAP complex: structural basis for GTPase activation and its loss in oncogenic Ras mutants. *Science* 1997;277: 333–8.
53. Ahmadian MR, Stege P, Scheffzek K, Wittinghofer A. Confirmation of the arginine-finger hypothesis for the GAP-stimulated GTP-hydrolysis reaction of Ras. *Nat Struct Biol* 1997;4:686–9.
54. Huang L, Hofer F, Martin GS, Kim SH. Structural basis for the interaction of Ras with RalGDS. *Nat Struct Biol* 1998;5:422–6.
55. Sun Q, Burke JP, Phan J, Burns MC, Olejniczak ET, Waterson AG, et al. Discovery of small molecules that bind to K-Ras and inhibit Sos-mediated activation. *Angew Chem Int Ed Engl* 2012;51:6140–3.
56. Lenzen C, Cool RH, Prinz H, Kuhlmann J, Wittinghofer A. Kinetic analysis by fluorescence of the interaction between Ras and the catalytic domain of the guanine nucleotide exchange factor Cdc25Mm. *Biochemistry* 1998; 37:7420–30.
57. Chen CC, Er TK, Liu YY, Hwang JK, Barrio MJ, Rodrigo M, et al. Computational analysis of KRAS mutations: implications for different effects on the KRAS p.G12D and p.G13D mutations. *PLoS ONE* 2013;8: e55793.
58. Smith MJ, Neel BG, Ikura M. NMR-based functional profiling of RASopathies and oncogenic RAS mutations. *Proc Natl Acad Sci U S A* 2013; 110:4574–9.
59. Bazan V, Agnese V, Corsale S, Calo V, Valerio MR, Latteri MA, et al. Specific TP53 and/or Ki-ras mutations as independent predictors of clinical outcome in sporadic colorectal adenocarcinomas: results of a 5-year Gruppo Oncologico dell'Italia Meridionale (GOIM) prospective study. *Ann Oncol* 2005;16(Suppl 4):iv50–5.
60. Ahmadian MR, Hoffmann U, Goody RS, Wittinghofer A. Individual rate constants for the interaction of Ras proteins with GTPase-activating proteins determined by fluorescence spectroscopy. *Biochemistry* 1997;36: 4535–41.
61. Bührman G, Kumar VS, Cirit M, Haugh JM, Mattos C. Allosteric modulation of Ras-GTP is linked to signal transduction through RAF kinase. *J Biol Chem* 2011;286:3323–31.

62. Vetter I, Linnemann T, Wohlgemuth S, Geyer M, Kalbitzer HR, Herrmann C, et al. Structural and biochemical analysis of Ras-effector signaling via RalGDS. *FEBS Lett* 1999;451:175–80.
63. Moodie SA, Paris M, Villafranca E, Kirshmeier P, Willumsen BM, Wolfman A. Different structural requirements within the switch II region of the Ras protein for interactions with specific downstream targets. *Oncogene* 1995; 11:447–54.
64. Buhrman G, Holzapfel G, Fetis S, Mattos C. Allosteric modulation of Ras positions Q61 for a direct role in catalysis. *Proc Natl Acad Sci U S A* 2010;107:4931–6.
65. Buhrman G, Wink G, Mattos C. Transformation efficiency of RasQ61 mutants linked to structural features of the switch regions in the presence of Raf. *Structure* 2007;15:1618–29.
66. Su F, Viros A, Milagre C, Trunzer K, Bollag G, Spleiss O, et al. RAS mutations in cutaneous squamous-cell carcinomas in patients treated with BRAF inhibitors. *N Engl J Med* 2012;366:207–15.
67. Cespedes MV, Sancho FJ, Guerrero S, Parreno M, Casanova I, Pavon MA, et al. K-ras Asp12 mutant neither interacts with Raf, nor signals through Erk and is less tumorigenic than K-ras Val12. *Carcinogenesis* 2006; 27:2190–200.

Molecular Cancer Research

Biochemical and Structural Analysis of Common Cancer-Associated KRAS Mutations

John C. Hunter, Anuj Manandhar, Martin A. Carrasco, et al.

Mol Cancer Res 2015;13:1325-1335. Published OnlineFirst June 2, 2015.

| | |
|-------------------------------|---|
| Updated version | Access the most recent version of this article at: doi: 10.1158/1541-7786.MCR-15-0203 |
| Supplementary Material | Access the most recent supplemental material at: http://mcr.aacrjournals.org/content/suppl/2015/06/04/1541-7786.MCR-15-0203.DC1.html |

| | |
|-----------------------|--|
| Cited articles | This article cites 64 articles, 24 of which you can access for free at: http://mcr.aacrjournals.org/content/13/9/1325.full.html#ref-list-1 |
|-----------------------|--|

| | |
|-----------------------------------|---|
| E-mail alerts | Sign up to receive free email-alerts related to this article or journal. |
| Reprints and Subscriptions | To order reprints of this article or to subscribe to the journal, contact the AACR Publications Department at pubs@aacr.org . |
| Permissions | To request permission to re-use all or part of this article, contact the AACR Publications Department at permissions@aacr.org . |